UC Berkeley
UC Berkeley Previously Published Works

Title

Two spatially separated phases in semiconducting Rb0.8Fe1.5S2

Permalink

https://escholarship.org/uc/item/2zx4f2rn

Journal

Physical Review B, 90(12)

ISSN

2469-9950

Authors

Wang, Meng
Tian, Wei
Valdivia, P
et al.

Publication Date

2014-09-01

DOI

10.1103/physrevb.90.125148

Peer reviewed

Two spatially separated phases in semiconducting Rb$_{0.8}$Fe$_{1.5}$S$_2$

Meng Wang,[1,*] Wei Tian,[2] P. Valdivia,[1] Songxue Chi,[2] E. Bourret-Courchesne,[3] Pengcheng Dai,[4,5] and R. J. Birgeneau[1,3,6]

[1]*Department of Physics, University of California, Berkeley, California 94720, USA*
[2]*Quantum Condensed Matter Division, Oak Ridge National Laboratory, Oak Ridge, Tennessee 37831-6393, USA*
[3]*Materials Science Division, Lawrence Berkeley National Laboratory, Berkeley, California 94720, USA*
[4]*Department of Physics and Astronomy, Rice University, Houston, Texas 77005, USA*
[5]*Institute of Physics, Chinese Academy of Sciences, P. O. Box 603, Beijing 100190, China*
[6]*Department of Materials Science and Engineering, University of California, Berkeley, California 94720, USA*

We report neutron scattering and transport measurements on semiconducting Rb$_{0.8}$Fe$_{1.5}$S$_2$, a compound isostructural and isoelectronic to the well-studied $A_{0.8}$Fe$_y$Se$_2$(A = K, Rb, Cs, Tl/K) superconducting systems. Both resistivity and dc susceptibility measurements reveal a magnetic phase transition at T = 275 K. Neutron diffraction studies show that the 275 K transition originates from a phase with rhombic iron vacancy order which exhibits an in-plane stripe antiferromagnetic ordering below 275 K. In addition, the stripe antiferromagnetic phase interdigitates mesoscopically with an ubiquitous phase with $\sqrt{5} \times \sqrt{5}$ iron vacancy order. This phase has a magnetic transition at T_N = 425 K and an iron vacancy order-disorder transition at T_S = 600 K. These two different structural phases are closely similar to those observed in the isomorphous Se materials. Based on the close similarities of the in-plane antiferromagnetic structures, moments sizes, and ordering temperatures in semiconducting Rb$_{0.8}$Fe$_{1.5}$S$_2$ and K$_{0.81}$Fe$_{1.58}$Se$_2$, we argue that the in-plane antiferromagnetic order arises from strong coupling between local moments. Superconductivity, previously observed in the $A_{0.8}$Fe$_y$Se$_{2-z}$S$_z$ system, is absent in Rb$_{0.8}$Fe$_{1.5}$S$_2$, which has a semiconducting ground state. The implied relationship between stripe and block antiferromagnetism and superconductivity in these materials as well as a strategy for further investigation is discussed in this paper.

I. INTRODUCTION

The $A_{0.8}$Fe$_{1.6\pm\delta}$Se$_2$ (A = K, Rb, Cs, Tl/K) materials, the so-called "245" systems, were discovered at the end of 2010 and have since generated a great deal of interest, in large part because of their unique properties: iron vacancy order, block antiferromagnetism (AF) with large $3.3\mu_B$ moments aligned along the c axis, and the existence of superconductivity for appropriate chemical compositions [1–6]. In the Fe pnictide systems, the parent compounds of the superconductors exhibit a collinear antiferromagnetic structure with small ordered moments, typically less than $1\mu_B$ [7–10]. Superconductivity arises upon electron or hole doping of the parent compounds, which concomitantly suppresses the AF order. Spin fluctuations associated with the AF order, which exist throughout the superconducting (SC) dome, are thought to play a crucial role in the mechanism of superconductivity [11–13]. In the standard interpretation, nesting between the hole and electron Fermi surfaces gives rise to spin-density-wave (SDW) order. In addition, the ubiquitous occurrence of a neutron "spin-resonance" at the SDW wave vector in superconducting iron pnictide compounds has been suggested to correlate with "$s\pm$" pairing symmetry [14–16].

A spin resonance mode was also found in the 245 system, but at a wave vector different from those of both the block and stripe AF orders [17,18]. Importantly, unlike the Fe pnictides, a weak electron-like Fermi pocket and hole-like bands below the Fermi surface are found in place of hole Fermi surfaces around the Γ point in the $A_{0.8}$Fe$_{1.6}$Se$_2$ system [19–21].

The occurrence of superconductivity with T_c up to 32 K in the 245 system in the absence of electron-hole nesting presents a significant challenge to current theories of these phenomena [22].

There is extensive empirical evidence that the SC phase occurs mesoscopically separated from the block AF insulator [23–29]. The block AF phase exists throughout the two-dimensional phase diagrams of A_xFe$_y$Se$_2$ over wide variations in the alkali metal ($0.77 \leqslant x \leqslant 0.98$) and iron contents ($1.48 \leqslant y \leqslant 1.65$), with little change of T_N [30]. We emphasize that (x,y) are for the sample as a whole, not the two separate constituent phases in most studies. The reports focused on the composition of the superconducting phase remain conflicting [27,31–33]. Thus, the nature of the real superconducting phase and its parent compound are still under debate [25–27,31–34]. Both theory and photoemission experiment proposed an insulating or semiconducting phase as a candidate for the parent compound of the superconducting phase in $(K,Tl)_x$Fe$_y$Se$_2$ [25,35]. Importantly, the same stripe AF structure with in-plane ordered moments that occurs in the parent compounds of pnictide superconductors was observed in semiconducting K$_{0.81}$Fe$_{1.58}$Se$_2$ by neutron diffraction [32]. If the stripe phase with in-plane AF order is, in fact, the parent compound of the superconducting phase in the 245 system, then the SC in this system may have the same underlying mechanism as that in the other iron-based superconductors, in spite of the absence of electron-hole nesting and different neutron spin resonance wave vectors [14–21]. Therefore, determining the origin of the in-plane AF order in the semiconducting phase and its relationship with superconductivity is crucial to understanding the mechanism of superconductivity in the A_xFe$_y$Se$_2$ system.

*wangm@berkeley.edu

The low-temperature electrical resistivity of the 245 system can be changed from insulating to semiconducting or superconducting by controlling the iron content as in $A_{0.8}Fe_ySe_2$, generally in concert with the alkali concentration A, or by substitution of sulfur on the selenium sites as in $A_{0.8}Fe_ySe_{2-z}S_z$ [32,36–40]. In studies to date, changing the iron content of the pure Se two-phase material results in the sudden disappearance of the superconductivity, while sulfur substitution for selenium appears to suppress superconductivity gradually, resulting in a semiconducting ground state [39]. Accordingly, semiconducting $A_{0.8}Fe_yS_2$ may also be viewed as the parent compound of the $A_{0.8}Fe_ySe_{2-z}S_z$ superconductors, although the magnetic phase diagram has not yet been determined for high sulfur substitution. Both high-temperature transport and Raman scattering measurements indicate that the block AF phase also exists in the $A_xFe_yS_2$ system [41,42]. Thus, it is important to investigate whether or not the in-plane AF order occurs in $A_{0.8}Fe_yS_2$ and, if so, to determine its relationships with superconductivity in the S-substituted $A_{0.8}Fe_ySe_{2-z}S_z$.

In this paper, we present transport and elastic neutron scattering measurements on single crystals of semiconducting $Rb_{0.8}Fe_{1.5}S_2$. Two magnetic phases are found in this material with the next-nearest (NN) Fe neighbor bond distances at 180 K 3.765 Å and 3.889 Å for the two phases, respectively. The first phase, the 245 phase, which has the more compact in-plane lattice constants, has the $\sqrt{5} \times \sqrt{5}$ iron vacancy order and block AF order as in the $A_{0.8}Fe_{1.6\pm\delta}Se_2$ system [30]. The Néel temperature of the block AF order is 425 K; this is reduced significantly compared with $\sim$560 K in $A_{0.8}Fe_ySe_2$ and is also well separated from the $\sqrt{5} \times \sqrt{5}$ iron-vacancy-ordering temperature of 600 K in $Rb_{0.8}Fe_{1.5}S_2$ [5]. Schematics of the three-dimensional structure together with that of the iron plane with ordered moments and iron vacancies are shown in Figs. 1(a) and 1(b). The second phase has rhombic iron vacancy order with in-plane stripe AF order below 275 K [Figs. 1(c) and 1(d)] [43]. We named it the "234" phase (this assumes an ideal stoichiometry $RbFe_{1.5}S_2$) in spite of the possible deviation of Rb in the discussion below. The estimated in-plane magnetic moment size of $(2.8 \pm 0.5)\mu_B$ and the Néel temperature of 275 K for the stripe AF order in semiconducting $Rb_{0.8}Fe_{1.5}S_2$ are surprisingly close to the $2.88\mu_B$ moments and $T_N = 280$ K of the stripe AF order in semiconducting $K_{0.81}Fe_{1.58}Se_2$ [32]. These results suggest that strong coupling of local moments plays the dominant role in the formation of in-plane AF order in semiconducting $A_{0.8}Fe_yX_2$ ($X =$ Se, S).

II. EXPERIMENTAL DETAILS

Our experiments were carried out on the HB-1A triple-axis spectrometer and HB-2C wide-angle neutron diffractometer (WAND) at the High-Flux Isotope Reactor, Oak Ridge National laboratory. The triple-axis experiment employed two pyrolytic graphite (PG) filters before the sample to reduce $\lambda/2$ contamination and horizontal collimation $40' - 40'$-$S - 40' - 80'$ with a fixed incident beam energy of $E_i = 14.64$ meV. A single piece of crystal weighing 220 mg with a mosaic of $1.5°$ was loaded into a closed-cycle refrigerator (CCR) which covers the temperature range from 30 to 750 K. The sample was aligned in the $[H, H, L]$ zone and the
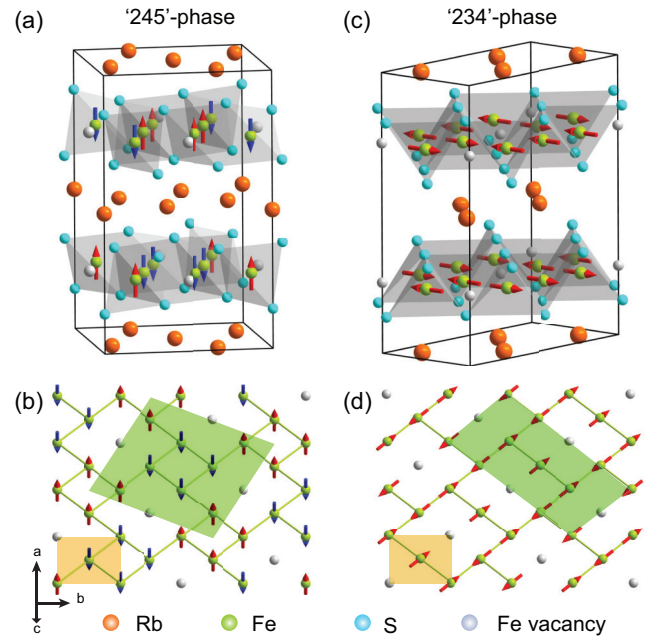

FIG. 1. (Color online) (a) Three-dimensional structure of the block AF phase in $Rb_{0.8}Fe_{1.5}S_2$. (b) The Fe plane of block AF phase with $\sqrt{5} \times \sqrt{5}$ iron order, where a magnetic unit cell with lattice parameter $a_s = \sqrt{5} \times 3.765$ Å has been marked as green. The tetragonal lattice cell used throughout this paper is shaded light orange. The red and blue arrows represent the out-of-plane spin directions up and down. The orange, lime, turquoise, and light gray balls are Rb, Fe, and S atoms and Fe vacancies, respectively. (c) A three-dimensional magnetic unit cell of the in-plane AF order and (d) Fe-plane with the rhombic iron vacancy order. A magnetic unit cell is shaded green. The diagonal Fe bonds are 3.889 Å at 180 K.

$[H, 3H, L]$ zone in tetragonal notation with lattice parameters $a = b = 3.889$ Å, $c = 13.889$ Å for the 234 phase and $a = b = 3.765$ Å, $c = 13.889$ Å for the 245 phase optimized at 180 K. The momentum transfer (q_x, q_y, q_z) is defined as $(2\pi H/a, 2\pi K/b, 2\pi L/c)$ in Å^{-1}. (H, K, L) are the Miller indices in reciprocal lattice units (r.l.u.). We labeled the wave vectors $Q = [H, K, L]$ r.l.u. throughout this paper. By employing the degrees of freedom of the upper and lower goniometers of HB-1A, we were able to probe wave vectors in the $[H, K]$ plane near $[H, H, L]$. A Ge(115) monochromator was used to produce a neutron beam with $\lambda = 1.482$ Å in the experiment at WAND. The one-dimensional ^{3}He detectors with 624 anodes can cover a wide range in reciprocal space by rotating the sample. A standard CCR was used to cover the temperature range between 4 and 300 K.

The $Rb_{0.8}Fe_{1.5}S_2$ single crystals were grown by the Bridgman method with a one-step reacting. Stoichiometric amounts of high purity of a Rb ingot, Fe powder, and pieces of S were loaded in an alumina crucible in an argon-gas-filled glove box; then the alumina crucible was sealed in a quartz tube under vacuum. The quartz tube was loaded into a box furnace and kept at 200 °C for 24 hours; then warmed up to 500 °C and held for 20 hours; heated slowly to 1050 °C for melting 5 hours; cooled down to 750 °C at a rate of 4 °C/hour; and finally cooled to room temperature. We obtained single crystals with dimensions up to $5 \times 5 \times 4$ mm^3.
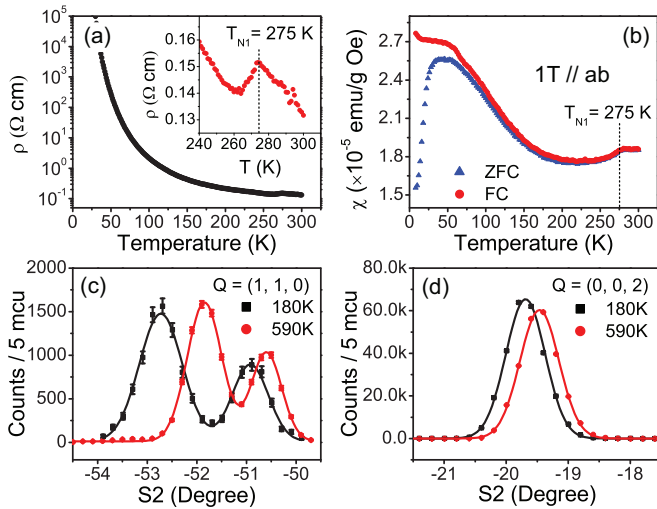
FIG. 2. (Color online) (a) In-plane resistivity measurement of semiconducting $Rb_{0.8}Fe_{1.5}S_2$. (b) 1 T zero-field-cooled (ZFC) and field-cooled (FC) dc magnetic susceptibility measurements with $H \parallel ab$ plane. A spin-glass-like behavior appears below 55 K. A kink corresponding to the stripe AF order transition is observed in both resistivity and susceptibility measurements at $T = 275$ K. (c) The well-separated peaks in the θ-2θ scans at nuclear reflection wave vector $Q = (1,1,0)$ demonstrate two different sets of in-plane lattice constants at 180 and 590 K. (d) θ-2θ scans at $Q = (0,0,2)$ show a single lattice constant c within the instrument resolution. The error bars are one standard deviation and solid lines are fits to a Gaussian function throughout this paper.

III. RESULTS

We characterized the transport properties of several $Rb_{0.8}Fe_{1.5}S_2$ single crystals with a Quantum Design Physical Property Measurement System (PPMS). The results were very consistent among the different samples measured and indicated consistent phases. The in-plane resistivity shown in Fig. 2(a) on a logarithm scale represents clear semiconducting behavior. This semiconducting characteristic is quite similar to that of the potassium compound with equivalent composition, $K_{0.8}Fe_{1.5}S_2$ [40]. These results reveal, as expected, that $Rb_{0.8}Fe_yS_2$ and $K_{0.8}Fe_yS_2$ have similar transport characteristics. The enlarged resistivity from 240 to 300 K in the inset of Fig. 2(a) implies a phase transition at 275 K. This transition temperature corresponds to the onset of the in-plane stripe AF order observed by neutron diffraction, which is discussed in more detail below. The kink at 275 K corresponding to the stripe AF transition can also be seen in the susceptibility measurement. The difference between the zero-field-cooled (ZFC) and field-cooled (FC) susceptibilities in Fig. 2(b) suggests the possibility of a spin-glass phase coincident with the long-range AF order in $Rb_{0.8}Fe_{1.5}S_2$, similar to that which has been proposed for $K_{0.88}Fe_{1.63}S_2$ [44].

The lattice constants can be optimized by carrying out θ-2θ scans at nuclear Bragg peaks: scanning the angle of the incident beam and exit beam $S2$ (2θ), and rotating the sample angle (θ) by half of the step. The two well-separated peaks in the scan at $Q = (1,1,0)$ are strong evidence for two structural phases existing in this sample [Fig. 2(c)]. As estimated from the integrated peak intensities at 180 K, the 245 phase with

$a = b = 3.765$ Å (peak centered at -52.70) has $\sim 65\%$ volume fraction, and the 234 phase with $a = b = 3.889$ Å (peak centered at -50.90) has $\sim 35\%$ volume fraction. We observed that the volume fractions of the two phases varied among our different samples [45]. The transition temperatures of each phase are consistent. The two phases have the same lattice constant $c = 13.889$ Å based on the θ-2θ scans at $Q = (0,0,2)$ at 180 K, as shown in Fig. 2(d). The peaks shift slightly due to the change of lattice constants at 590 K, but the peaks at $Q = (1,1,0)$ are still clearly distinguishable at 590 K [45]. This is in marked contrast with the behavior in phase-separated superconducting $K_{0.8}Fe_{1.6}Se_2$, where the nonmagnetic phase with the more compact in-plane lattice constant merges together with the block AF phase at temperatures above the iron-vacancy order-disorder transition at 520 K [23,33].

We first discuss the 245 phase, which has the block AF order and $\sqrt{5} \times \sqrt{5}$ iron vacancy order in Figs. 1(a) and 1(b). The block AF order generates magnetic peaks at the wave vectors shown as the solid circles in the $[H, K]$ scattering planes for $L =$ odd in the inset figure of Fig. 3(b). The $\sqrt{5} \times \sqrt{5}$ iron vacancy order produces nuclear peaks at the positions of the blank squares in the $[H, K]$ planes for $L =$ even. The wave vectors connected by red and blue lines in the inset of Fig. 3(b) originate from the left and right chiralities, respectively. The details of the diffraction have been described elsewhere [29]. By comparing the peak centers under the two sets of lattice constants, the set with $a = b = 3.765$ Å was determined to correspond to the block AF phase. Figures 3(a)–3(c) represent scans at the magnetic wave vectors of $Q = (0.2, 0.4, 1)$, $Q = (0.2, 0.4, 3)$, and $Q = (1.2, 1.4, 1)$ at 212 K. The dramatic decrease of the magnetic peak intensity at $L = 3$ compared with that at $L = 1$ is consistent with c-axis-aligned moments together with the Fe^{2+} magnetic form factor. Figure 3(a) also shows a scan at the equivalent wave vector $Q = (0.4, 0.2, 1)$ from the other chirality. The temperature dependence of the rocking-curve scans demonstrates that the Néel temperature is approximately 425 K, which is significantly lower than that in the $A_{0.8}Fe_ySe_2$ system [5]. The fingerprint reflection peaks of the $\sqrt{5} \times \sqrt{5}$ iron vacancy order at $Q = (0.2, 0.6, 2)$ and $Q = (0.4, 0.8, 2)$ were also investigated and are represented in Figs. 3(e) and 3(f). The order-disorder transition temperature of the iron vacancies occurs at 600 K. Here we have carried out θ-2θ scans in order to track the temperature dependence of the iron vacancy order, while accounting for thermal expansion.

Figure 4 summarizes the Bragg peaks of the 234 phase associated with the in-plane stripe AF order and rhombic iron vacancy order. The magnetic peaks are accurately centered at the wave vectors $Q = (0.5, 0.5, L = 1, 3, 5)$ at 180 K with lattice constants $a = b = 3.889$ Å, $c = 13.889$ Å. The magnetic peaks disappear completely by 280 K. The rhombic iron vacancy order together with the stripe AF order will induce magnetic peaks at $Q = (0.25, 0.25, L =$ odd), $Q = (0.75, 0.75, L =$ odd); and nuclear peaks at $Q = (0.25, 0.75, L =$ even), $Q = (0.75, 0.25, L =$ even), $Q = (0.5, 0.5, L =$ even), as demonstrated in the inset of Fig. 4(d). We show reflection peaks in the $[H, 3H, L]$ plane in Fig. 4(e) at 6 K and in Fig. 4(f) at 280 K. The peaks centered at $Q = (0.25, 0.75, L)$, $Q = (0.5, 0.5, L)$, and $Q = (0.75, 2.25, L)$, $L = 0, -2, -4$ are consistent with the
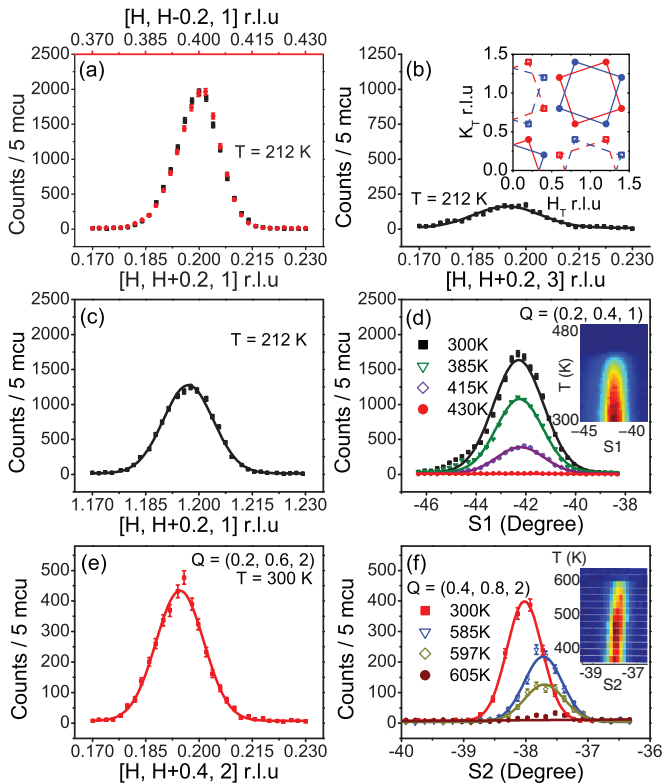
FIG. 3. (Color online) Magnetic and nuclear reflection peaks associated with the block AF phase and $\sqrt{5} \times \sqrt{5}$ iron vacancy order. Scans through magnetic peaks at (a) $Q = (0.2, 0.4, 1)$, (b) $Q = (0.2, 0.4, 3)$, and (c) $Q = (1.2, 1.4, 1)$ along the $[H, H + 0.2]$ direction at $T = 212$ K. The red solid points in panel (a) through $Q = (0.4, 0.2, 1)$ are from the other chirality. (d) Rocking-curve scans through magnetic peak $Q = (0.2, 0.4, 1)$ at selected temperatures of $T = 300, 385, 415,$ and 430 K. (e) Scan through the nuclear peak at $Q = (0.2, 0.6, 2)$ along the $[H, H + 0.4]$ direction associated with the $\sqrt{5} \times \sqrt{5}$ iron vacancy order at $T = 300$ K. (f) θ-2θ scans through nuclear peak at $Q = (0.4, 0.8, 2)$ at $T = 300, 585, 597,$ and 605 K. The inset in panel (b) is the expected magnetic Bragg peaks (solid circles, $L =$ odd) and nuclear Bragg peaks (open squares, $L =$ even) in tetragonal reciprocal space. The red and blue lines indicate two different chiralities. The insets in panels (d) and (f) are color maps of the temperature dependence of reflection peaks corresponding to panels (d) and (f).
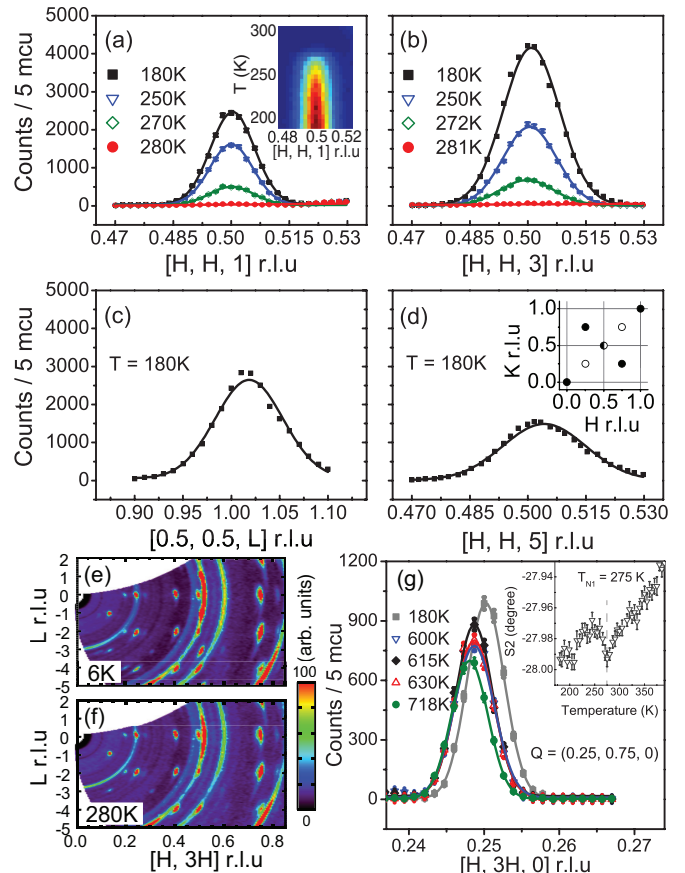
FIG. 4. (Color online) Diffraction studies of the in-plane AF phase with rhombic iron vacancy order. Scans of magnetic peaks at wave vector of (a) $Q = (0.5, 0.5, 1)$, (b) $Q = (0.5, 0.5, 3)$, (d) $Q = (0.5, 0.5, 5)$ along the $[H, H]$ direction, and (c) $Q = (0.5, 0.5, 1)$ along L direction at selected temperatures. The inset of panel (a) is a color map of detailed temperature dependence. Panels (e) and (f) show the nuclear peaks at the wave vectors of $H = 0.25, 0.5, 0.75;$ $L =$ even and magnetic peaks at $H = 0.5, L =$ odd from the in-plane AF phase in the $[H, 3H, L]$ plane at 6 and 280 K, respectively. The nuclear peaks were not changed, but the magnetic peaks disappeared at 280 K. The peaks at $H = 0.4, L =$ even originate from the $\sqrt{5} \times \sqrt{5}$ iron vacancy order in the block AF phase. (g) Scans along $[H, 3H, 0]$ r.l.u. at peaks of the rhombic iron vacancy order at $Q = (0.25, 0.75, 0)$ at 180 K, 600 K, 615 K and 630 K. The evolution of 2θ ($S2$) of the peak centers versus temperature indicates an in-plane lattice constant change across the in-plane magnetic structure transition in the inset of (g).

rhombic iron vacancy order. The magnetic peak at $Q = (0.5, 1.5, 3)$ at 6 K in Fig. 4(e) disappears at a temperature above $T_N = 275$ K. The peaks at $Q = (0.4, 1.2, L = 0, -2, -4)$ originate from the $\sqrt{5} \times \sqrt{5}$ iron vacancy order of the 245 phase. The temperature dependence of the θ-2θ scans in Fig. 4(g) shows the existence of the rhombic iron vacancy order at temperatures as high as 718 K; this is the reason the two phases did not merge together at the temperature above the iron vacancy order-disorder transition at $T_S = 600$ K of the 245 phase in $\mathrm{Rb_{0.8}Fe_{1.5}S_2}$ [23,33]. From the inset, one can see a clear anomaly in the temperature dependence of the in-plane lattice constant at the AF transition indicating strong coupling between the structure and the antiferromagnetism. Residual peaks with temperature-independent intensities were observed at the magnetic peak positions above

T_N in semiconducting $\mathrm{K_{0.81}Fe_{1.58}Se_2}$ [32]. However, we did not observe residual intensity at these positions above T_N in our semiconducting $\mathrm{Rb_{0.8}Fe_{1.5}S_2}$ single crystals. This significant difference in these two systems, which otherwise behave quite similarly, remains to be understood.

In order to determine the transition temperatures of the 234 and 245 phases in $\mathrm{Rb_{0.8}Fe_{1.5}S_2}$, we carefully measured the intensities of the fingerprint reflection peaks versus temperature; the results are shown in Fig. 5. The Néel temperature of the in-plane stripe AF order of $T_{N1} = 275$ K in the 234 phase of semiconducting $\mathrm{Rb_{0.8}Fe_{1.5}S_2}$ is very close to $T_N = 280$ K of the stripe AF order in semiconducting $\mathrm{K_{0.81}Fe_{1.58}Se_2}$ [32].
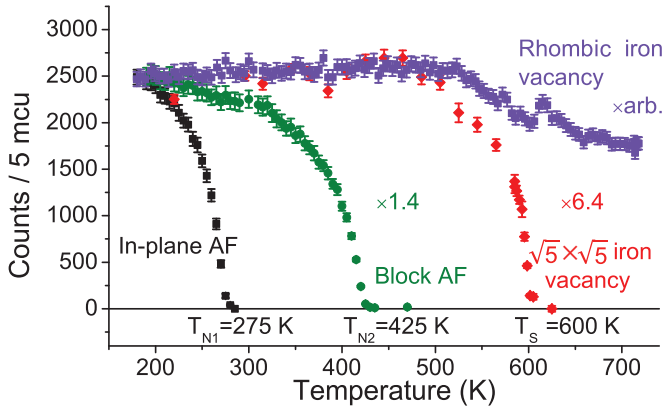
FIG. 5. (Color online) Temperature dependence of order parameters for the in-plane stripe AF, the rhombic iron vacancy, the block AF and the $\sqrt{5} \times \sqrt{5}$ iron vacancy orders. The height of peaks at $Q = (0.5, 0.5, 1)$ fit from $[H, H]$ scans shown as the black squares represent the stripe AF transition at $T_{N1} = 275$ K. The temperature dependence of peak height at $Q = (0.2, 0.4, 1)$ (green circle) fit from rocking-curve scans shows the block AF transition at $T_{N2} = 425$ K. The red diamonds obtained from θ-2θ scans through $Q = (0.4, 0.8, 2)$ indicate a first-order-like transition of the $\sqrt{5} \times \sqrt{5}$ iron vacancies at $T_S = 600$ K. The rhombic iron vacancy order parameter integrated from the θ-2θ scans at $Q = (0.25, 0.75, 0)$ was collected from another piece of single crystal with the same composition aligned in the $[H, 3H, L]$ zone.

The block AF order of the 245 phase has a Néel temperature at $T_{N2} = 425$ K and an iron vacancy ordering temperature of $T_S = 600$ K. These have a much larger separation than those in the $A_{0.8}\text{Fe}_y\text{Se}_2$ system [5,6].

IV. DISCUSSIONS AND CONCLUSIONS

The similarity of the Néel temperatures suggests the crucial role of local moment superexchange interactions between the iron spins. Thus, we propose that strong correlation effects are essential to the formation of the stripe AF phase, in contrast with the spin-density-wave mechanism, which has been proposed as the origin of the magnetic order in the parent compounds of the iron pnictide superconductors [14,15]. The strong-coupling scenario can also be reconciled with the absence of hole Fermi surfaces in $A_{0.8}\text{Fe}_y\text{Se}_2$ [19–21]. Similar to the iron pnictides, the spin-resonance modes associated with superconductivity in iron chalcogenide ($\text{FeTe}_{1-x}\text{Se}_x$ and $A_{0.8}\text{Fe}_y\text{Se}_2$) systems are compatible with nesting between the hole-electron or electron-electron Fermi surfaces [18]. In contrast with the pnictides, the in-plane magnetic orders in the iron chalcogenides are not compatible with nesting. The iron chalcogenides also have much larger local moments than the pnictide systems. The moments in the former are strongly suggestive of a localized rather than itinerant model for the magnetism.

The data in Fig. 5 show a surprising feature which indicates that the two different structural phases are in communication with each other. Specifically, there is a small increase ($\sim$10%) with increasing temperature in the intensity of the superlattice reflection associated with the rhombic vacancy order at the temperature at which the vacancies in the $\sqrt{5} \times \sqrt{5}$ phase be-

come disordered. The increase in the integrated intensity is also confirmed by the scans at $Q = (0.25, 0.75, 0)$, $T = 600, 615$, and 630 K in Fig. 4(g). The intensity change suggests that the iron, partially occupied on the rhombic vacancy sites of the 234 phase below $T_S = 600$ K, moves to the iron vacancy disordered 245 phase. The movement of iron vacancies between the two phases in $\text{Rb}_{0.8}\text{Fe}_{1.5}\text{S}_2$ suggests a possible way to understand the complex relationship between the AF structures and the superconductivity in the $A_{0.8}\text{Fe}_y\text{Se}_2$ system. In the compounds with net composition $A_{0.8}\text{Fe}_y\text{Se}_2$ ($1.5 < y < 1.6$), the material stabilized is a combination of the semiconducting phase $A_x\text{Fe}_{1.5\pm\delta}\text{Se}_2$ (234 phase) with in-plane stripe AF order and rhombic iron vacancy order together with the insulating phase, $A_{0.8}\text{Fe}_{1.6\pm\delta}\text{Se}_2$ (245 phase) with the block AF order and $\sqrt{5} \times \sqrt{5}$ iron vacancy order. By adding more iron, only the volume fraction of the two phases is changed; that is, one traverses a first-order two-phase coexistence region between the 234 and 245 phases. This explains naturally why the Néel temperature of the in-plane stripe AF order is so stable. The block AF phase with $\sqrt{5} \times \sqrt{5}$ iron vacancy order, $A_{0.8}\text{Fe}_{1.6\pm\delta}\text{Se}_2$ (245 phase), with $\delta = 0$, represents an endpoint of the two-phase coexistence region. In this picture, by further increasing the iron content beyond $y = 1.6$, the material then separates into a new iron rich superconducting, nonmagnetic phase, and the block AF phase with $\sqrt{5} \times \sqrt{5}$ iron vacancy order. We speculate that the 245 phase is a stable stoichiometric phase and that the $\sqrt{5} \times \sqrt{5}$ ordered iron vacancies cannot be readily occupied. This means that increasing the Fe content above 1.6 causes the formation of a new iron-rich phase which exhibits superconductivity. Concomitantly, the iron-rich SC phase is always accompanied by the 245 phase but the 245 phase is not the parent compound of the superconducting phase.

The results reported in this paper suggest a new strategy for probing the onset of superconductivity in the $A_x\text{Fe}_y\text{Se}_2$-type systems. In the pnictide systems, important insights have been gained by continuously tuning variables, such as the electron concentration by substitution (e.g., replacing Fe by Co or Ni) and thereby studying the evolution of the magnetism from the AF parent material to the superconducting material [11]. This is especially important at the onset of superconductivity where rich magnetic and superconducting behavior is observed. This approach does not seem to be possible in the $A_x\text{Fe}_y\text{Se}_2$ systems since the superconductivity seems to appear discontinuously. Yet it is clear from the results reported here that systematic variation of the S content in the $A_{0.8}\text{Fe}_y\text{Se}_{2-z}\text{S}_z$ system should enable one to study the continuous evolution from the "parent" stripe AF sulphide to the superconducting mixed sulphide-selenide thus emulating studies in pnictide materials like those in $\text{BaFe}_2\text{As}_{2-x}\text{P}_x$ [46]. The $A_{0.8}\text{Fe}_y\text{Se}_{2-z}\text{S}_z$ system may be closely analogous to the $\text{BaFe}_2\text{As}_{2-x}\text{P}_x$ system.

In summary, we have studied the magnetic and nuclear structures of semiconducting $\text{Rb}_{0.8}\text{Fe}_{1.5}\text{S}_2$ single crystals. Similar to semiconducting $\text{K}_{0.81}\text{Fe}_{1.58}\text{Se}_2$, there is an in-plane stripe AF phase with rhombic iron vacancy order, in addition to the block AF phase with $\sqrt{5} \times \sqrt{5}$ iron vacancy order. The robust $(2.8 \pm 0.5)\mu_B$ in-plane ordered moments and $\sim$280 K Néel temperature of the stripe AF phase in semiconducting Fe-Se and Fe-S based systems suggest that strong electronic correlations play a dominant role in determining the nature of

the magnetic state. The relationships between the block AF phase, the superconducting phase, and the in-plane stripe AF phase have been discussed in this paper. The $A_{0.8}Fe_ySe_{2-z}S_z$ system opens a new window to study the relationship between the antiferromagnetism and the superconductivity.

ACKNOWLEDGMENTS

[1] J. G. Guo, S. F. Jin, G. Wang, S. C. Wang, K. X. Zhu, T. T. Zhou, M. He, and X. L. Chen, Phys. Rev. B **82**, 180520(R) (2010).

[2] A. Krzton-Maziopa, Z. Shermadini, E. Pomjakushina, V. Pomjakushin, M. Bendele, A. Amato, R. Khasanov, H. Luetkens, and K. Conder, J. Phys.: Condens. Matter **23**, 052203 (2011).

[3] M. H. Fang, H. D. Wang, C. H. Dong, Z. J. Li, C. M. Feng, J. Chen, and H. Q. Yuan, Europhys. Lett. **93**, 47004 (2011).

[4] A. F. Wang, J. J. Ying, Y. J. Yan, R. H. Liu, X. G. Luo, Z. Y. Li, X. F. Wang, M. Zhang, G. J. Ye, P. Cheng, Z. J. Xiang, and X. H. Chen, Phys. Rev. B **83**, 060512 (2011).

[5] W. Bao, Q. Huang, G. F. Chen, M. A. Green, D. M. Wang, J. B. He, X. Q. Wang, and Y. Qiu, Chin. Phys. Lett. **28**, 086104 (2011).

[6] F. Ye, S. Chi, W. Bao, X. F. Wang, J. J. Ying, X. H. Chen, H. D. Wang, C. H. Dong, and M. H. Fang, Phys. Rev. Lett. **107**, 137003 (2011).

[7] C. de la Cruz, Q. Huang, J. W. Lynn, J. Li, W. Ratcliff II, J. L. Zarestky, H. A. Mook, G. F. Chen, J. L. Luo, N. L. Wang, and P. C. Dai, Nature (London) **453**, 899 (2008).

[8] Q. Huang, Y. Qiu, W. Bao, M. A. Green, J. W. Lynn, Y. C. Gasparovic, T. Wu, G. Wu, and X. H. Chen, Phys. Rev. Lett. **101**, 257003 (2008).

[9] S. L. Li, C. de la Cruz, Q. Huang, G. F. Chen, T. L. Xia, J. L. Luo, N. L. Wang, and P. C. Dai, Phys. Rev. B **80**, 020504(R) (2009).

[10] J. W. Lynn and Pengcheng Dai, Physica C (Amsterdam, Neth.) **469**, 469 (2009).

[11] D. C. Johnston, Adv. Phys. **59**, 803 (2010).

[12] P. C. Dai, J. P. Hu, and E. Dagotto, Nat. Phys. **8**, 709 (2012).

[13] M. Wang, C. Zhang, X. Lu, G. Tan, H. Luo, Y. Song, M. Wang, X. Zhang, E. A. Goremychkin, T. G. Perring, T. A. Maier, Z. Yin, K. Haule, G. Kotliar, and P. Dai, Nat. Commun. **4**, 2874 (2013).

[14] J. Dong *et al.*, Europhys. Lett. **83**, 27006 (2008).

[15] I. I. Mazin, D. J. Singh, M. D. Johannes, and M. H. Du, Phys. Rev. Lett. **101**, 057003 (2008).

[16] T. A. Maier and D. J. Scalapino, Phys. Rev. B **78**, 020514 (2008).

[17] J. T. Park, G. Friemel, Yuan Li, J.-H. Kim, V. Tsurkan, J. Deisenhofer, H.-A. Krug von Nidda, A. Loidl, A. Ivanov, B. Keimer, and D. S. Inosov, Phys. Rev. Lett. **107**, 177005 (2011).

[18] G. Friemel, J. T. Park, T. A. Maier, V. Tsurkan, Yuan Li, J. Deisenhofer, H. A. Krug von Nidda, A. Loidl, A. Ivanov, B. Keimer, and D. S. Inosov, Phys. Rev. B **85**, 140511(R) (2012).

[19] Y. Zhang, L. X. Yang, M. Xu, Z. R. Ye, F. Chen, C. He, J. Jiang, B. P. Xie, J. J. Ying, X. F. Wang, X. H. Chen, J. P. Hu, and D. L. Feng, Nat. Mater. **10**, 273 (2011).

[20] T. Qian, X.-P. Wang, W.-C. Jin, P. Zhang, P. Richard, G. Xu, X. Dai, Z. Fang, J.-G. Guo, X.-L. Chen, and H. Ding, Phys. Rev. Lett. **106**, 187001 (2011).

[21] D. X. Mou *et al.*, Phys. Rev. Lett. **106**, 107001 (2011).

[22] E. Dagotto, Rev. Mod. Phys. **85**, 849 (2013).

[23] A. Ricci, N. Poccia, B. Joseph, G. Arrighetti, L. Barba, J. Plaisier, G. Campi, Y. Mizuguchi, H. Takeya, Y. Takano, N. L. Saini, and A. Bianconi, Supercond. Sci. Technol. **24**, 082002 (2011).

[24] A. Ricci *et al.*, Phys. Rev. B **84**, 060511(R) (2011).

[25] F. Chen *et al.*, Phys. Rev. X **1**, 021020 (2011).

[26] W. Li, H. Ding, Z. Li, P. Deng, K. Chang, K. He, S. Ji, L. Wang, X. Ma, J. P. Hu, X. Chen, and Q. K. Xue, Phys. Rev. Lett. **109**, 057003 (2012).

[27] W. Li, H. Ding, P. Deng, K. Chang, C. Song, K. He, L. Wang, X. M, J. Hu, X. Chen, and Q. Xue, Nat. Phys. **8**, 126 (2012).

[28] Z. Wang, Y. J. Song, H. L. Shi, Z. W. Wang, Z. Chen, H. F. Tian, G. F. Chen, J. G. Guo, H. X. Yang, and J. Q. Li, Phys. Rev. B **83**, 140505(R) (2011).

[29] M. Wang *et al.*, Phys. Rev. B **84**, 094504(R) (2011).

[30] W. Bao, G. N. Li, Q. Huang, G. F. Chen, J. B. He, D. M. Wang, M. A. Green, Y. M. Qiu, J. L. Luo, and M. M. Wu, Chin. Phys. Lett. **30**, 027402 (2013).

[31] N. Lazarević, M. Abeykoon, P. W. Stephens, H. Lei, E. S. Bozin, C. Petrovic, and Z. V. Popović, Phys. Rev. B **86**, 054503 (2012).

[32] J. Zhao, H. Cao, E. Bourret-Courchesne, D. H. Lee, and R. J. Birgeneau, Phys. Rev. Lett. **109**, 267003 (2012).

[33] S. V. Carr, D. Louca, J. Siewenie, Q. Huang, A. F. Wang, X. H. Chen, and P. C. Dai, Phys. Rev. B **89**, 134509 (2014).

[34] X. X. Ding, D. L. Fang, Z. Y. Wang, H. Yang, J. Z. Liu, Q. Deng, G. B. Ma, C. Meng, Y. H. Hu, and Hai-Hu Wen, Nat. Commun. **4**, 1897 (2013).

[35] R. Yu, J. X. Zhu, and Q. Si, Phys. Rev. Lett. **106**, 186401 (2011).

[36] D. M. Wang, J. B. He, T. L. Xia, and G. F. Chen, Phys. Rev. B **83**, 132502 (2011).

[37] J. G. Guo, X. L. Chen, G. Wang, S. F. Jin, T. T. Zhou, and X. F. Lai, Phys. Rev. B **85**, 054507 (2012).

[38] K. F. Wang, H. C. Lei, and C. Petrovic, Phys. Rev. B **84**, 054526 (2011).

[39] H. C. Lei, M. Abeykoon, E. S. Bozin, K. F. Wang, J. B. Warren, and C. Petrovic, Phys. Rev. Lett. **107**, 137002 (2011).

[40] Y. Cai, Z. Wang, Z. W. Wang, Z. A. Sun, H. X. Yang, H. F. Tian, C. Ma, B. Zhang, and J. Q. Li, Europhys. Lett. **103**, 37010 (2013).

[41] J. J. Ying, Z. J. Xiang, Z. Y. Li, Y. J. Yan, M. Zhang, A. F. Wang, X. G. Luo, and X. H. Chen, Phys. Rev. B **85**, 054506 (2012).

[42] N. Lazarević, H. Lei, C. Petrovic, and Z. V. Popović, Phys. Rev. B **84**, 214305 (2011).

[43] H. Sabrowsky, M. Rosenberg, D. Welz, P. Deppe, and Schäfer, J. Magn. Magn. Mater. **54–57**, 1497 (1986).

[44] H. C. Lei, M. Abeykoon, E. S. Bozin, and C. Petrovic, Phys. Rev. B **83**, 180503(R) (2011).

[45] The θ-2θ scan at $Q = (1, 1, 0)$ on another piece of single crystal indicated $45 \pm 5\%$ 245 phase and $55 \pm 5\%$ 234 phase. The $(1,1,0)$ peaks from the two phases are separated as high as 718 K. Our neutron powder diffraction refinement on a 2 g sample ground by single crystals revealed that only 2% 245 phase and 98% 234 phase in the sample at 500 K.

[46] S. Kasahara, T. Shibauchi, K. Hashimoto *et al.*, Phys. Rev. B **81**, 184519 (2010).